LAWRENCE
LIVERMORE
NATIONAL
LABORATORY

LLNL-JRNL-420385

Constraints on the Formation Age of Cometary Material from the NASA Stardust Mission

J. Matzel, H. Ishii, D. Joswiak, I. Hutcheon, J. Bradley, D. Brownlee, P. K. Weber, N. Teslich, G. Matrajt, K. McKeegan, G. MacPherson

November 18, 2009

Science

Disclaimer

Constraints on the Formation Age of Cometary Material from the NASA Stardust Mission

J. E. P. Matzel[1,2*], H. A. Ishii[1], D. Joswiak[3], I. D. Hutcheon[1,2], J. P. Bradley[1], D. Brownlee[3], P. K. Weber[2], N. Teslich[1], G. Matrajt[3], K. D. McKeegan[4], and G. J. MacPherson[5].

[1]Institute of Geophysics and Planetary Physics, Lawrence Livermore National Laboratory, 7000 East Avenue, Livermore, CA 94550 USA.
[2]Glenn T. Seaborg Institute, Lawrence Livermore National Laboratory, 7000 East Avenue, Livermore, CA 94550 USA.
[3]Department of Astronomy, Box 351580, Univ. of Washington, Seattle, WA 98195 USA.
[4]Department of Earth and Space Sciences, Univ. of California, Los Angeles, CA 90095 USA.
[5]Department of Mineral Sciences, National Museum of Natural History, MRC-119, Smithsonian Institution, Washington, D.C. 20560 USA.
*To whom correspondence should be addressed. E-mail: matzel2@llnl.gov.

LLNL-JRNL-420385

ABSTRACT

We measured the ^{26}Al-^{26}Mg isotope systematics of a ~5μm refractory particle, Coki, returned from comet 81P/Wild 2 in order to relate the timescales of formation of cometary inclusions to their meteoritic counterparts. The data show no evidence of radiogenic ^{26}Mg and define an upper limit to the abundance of ^{26}Al at the time of particle formation of ^{26}Al/^{27}Al <1x10^{-5}. The absence of ^{26}Al indicates Coki formed >1.7 Ma after the oldest solar system solids, Ca-Al-rich inclusions (CAIs). The data presented here suggest that high temperature inner solar system material formed, was subsequently transferred to the Kuiper Belt, and incorporated into comets several million years following CAI formation.

The Stardust mission to comet 81P/Wild 2 was designed around the premise that comets preserve pristine remnants of the material from which the solar system formed, and in 2006, Stardust returned the first samples from a comet. The mission was expected to provide a unique window into the early solar system by returning a mix of solar system condensates, amorphous grains from the interstellar medium, and true stardust – crystalline grains originating in distant stars. Initial results, however, indicate that comet Wild 2 instead contains an abundance of high-

temperature silicate and oxide minerals analogous to minerals in carbonaceous chondrites (*1-5*). The detection of Wild 2 particles that resemble Ca-Al-rich inclusions (CAIs) (*6*) is particularly significant because CAIs were most plausibly created within one astronomical unit of the infant Sun (*7*) and are the oldest objects formed in the solar nebula (*8*). The presence of inner solar system material in comet Wild 2 (*1-3, 9*) underscores the importance of radial transport of material over large distances in the early solar nebula and raises key questions regarding the timescale of formation of comets and the relationship between comet Wild 2 and other primitive solar nebula objects.

With a half-life of 0.73 Ma, the decay of the short-lived radionuclide ^{26}Al to ^{26}Mg provides a high resolution, relative chronometer for events occurring during the first several million years of solar system history. Assuming a homogeneous initial distribution of ^{26}Al within the solar nebula (*10*), differences in the inferred initial ^{26}Al/^{27}Al can be ascribed to the passage of time. Most CAIs contain radiogenic ^{26}Mg due to the in situ decay of ^{26}Al (*10*). CAIs that contain little to no radiogenic ^{26}Mg fall primarily into two categories: 1) highly refractory grains (e.g. *11*) and rare FUN inclusions, named for their Fractionation and Unidentified Nuclear isotopic effects, which are believed to have formed very early (*12*); and 2) CAIs that show clear petrographic evidence for later reprocessing (*10*).

We applied the ^{26}Al-^{26}Mg isotope system to a recently discovered refractory particle from comet Wild 2 (C2061,3,141,0,0 – hereafter Coki). Coki contains no detectable radiogenic ^{26}Mg, strongly suggestive of late formation at least 1.7 Ma after most CAIs. The ^{26}Al-^{26}Mg data from Coki provide an important constraint on the accretion time scale of comets like Wild 2 and the timing of radial mixing of thermally-processed, high-temperature materials from the inner solar system to the outer reaches of the solar nebula.

Coki is a ~5 μm diameter polycrystalline refractory particle, likely a fragment of a once much larger particle (*13*), composed mostly of anorthite with minor calcic pyroxene and an Al-Si-rich glass occurring around the edge of the particle (Fig. 1). The glass may be due to melting experienced by the particle during capture into the Stardust silica aerogel collector. Small (<200 nm) spinel crystals are enclosed in glass and anorthite. The abundance of anorthite and absence of melilite (either within the Coki particle or anywhere along its deceleration track) suggest Coki most closely resembles a minor class of CAIs (type C) or plagioclase-rich chondrules (*6, 14-15*). Coki pyroxene compositions are Ti-rich and Fe-, Cr-poor (Figs. 2 and S1, Table S1) relative to pyroxene commonly found in plagioclase-rich chondrules (e.g. *14*), suggesting Coki may be most comparable to type C CAIs. Both type C CAIs and plagioclase-rich chondrules show clear petrographic evidence for complex multi-stage histories, including melting of refractory precursor materials and assimilation of late-stage metamorphic minerals in the chondrite-forming region (*6, 14-16*).

We measured the Mg isotope composition of Coki anorthite using the Cameca NanoSIMS 50 at Lawrence Livermore National Laboratory (*17*) on a ~3 μm diameter by 0.1 μm thick, electron transparent section mapped by transmission electron microscopy energy-dispersive spectroscopy (TEM/EDS) (Fig. 1). The section was prepared for NanoSIMS analysis using a focused ion beam instrument to deposit a Pt support film behind the Coki section and to remove interfering Mg-rich minerals (*17*). We simultaneously collected four ion images corresponding to $^{24}Mg^+$, $^{25}Mg^+$, $^{26}Mg^+$ and $^{27}Al^+$ secondary ions. The ion images were subdivided into three spatially continuous regions based on the $^{27}Al/^{24}Mg$ ratio, and Mg isotope ratios were calculated by summing the total ion intensity of each isotope over each region (SOM, Table 1).

The Mg isotope composition of Coki anorthite is indistinguishable from that of the terrestrial plagioclase standards. We find no evidence in Coki for either radiogenic ^{26}Mg from the decay of ^{26}Al or mass-dependent fractionation of Mg isotopes (Table 1, Fig. 3). The upper limit for the

initial abundance of ^{26}Al at the time Coki crystallized is $^{26}Al/^{27}Al < 1x10^{-5}$ based on the 2σ upper bound to the slope of a line fitted to the data. The absence of significant mass-dependent fractionation of Mg isotopes indicates that Coki is not a member of the rare group of CAIs known as FUN inclusions (*12*).

The ^{26}Al-^{26}Mg isotope systematics of primitive solar system materials establish a framework for the interpretation of the Coki Al-Mg data. The initial abundance of ^{26}Al in CAIs provides the anchor point for the ^{26}Al-^{26}Mg chronometer; the ^{26}Al-^{26}Mg record of CAIs and chondrules is best explained by formation in an isotopically homogeneous nebular reservoir characterized by an initial $^{26}Al/^{27}Al$ ratio of $\sim 5x10^{-5}$ (*10*). Recent high-precision studies of ^{26}Al in CAIs (*18-19*) and chondrules (*20*) support the inference of a uniform initial distribution of $^{26}Al/^{27}Al$ in the solar nebula and a very short time interval (<20 ka) for the primary crystallization of CAIs. Type C CAIs and chondrules, with initial $^{26}Al/^{27}Al << 5x10^{-5}$, typically show textural and mineralogical evidence for extensive melting of precursor materials (e.g. *21*), consistent with the absence of ^{26}Al. The ^{26}Al-^{26}Mg record of plagioclase-rich chondrules indicates that the time interval between CAI formation and the onset of chondrule formation is approximately one million years (*22-23*) and that transient events capable of producing high-temperature nebular components in the inner solar system persisted for close to 4 million years (*24-26*).

Our determination that Coki formed with an initial $^{26}Al/^{27}Al < 1x10^{-5}$ indicates that Coki crystallized at least 1.7 million years after the onset of CAI formation. This value is consistent with data for type C CAIs and plagioclase-rich chondrules that typically yield initial $^{26}Al/^{27}Al \leq 1x10^{-5}$ (*24 and references therein, 27*). The lack of ^{26}Al in some highly refractory phases (e.g. hibonite (e.g. *11*)) has been interpreted as very early formation prior to the incorporation or homogenization of ^{26}Al in the accretion disk. However, the petrography and mineral compositions of Coki are inconsistent with formation as very early condensates. The lack of ^{26}Al in Coki is also unlikely due to later redistribution of radiogenic ^{26}Mg either on Comet Wild 2 or

during capture in aerogel. The poorly consolidated and fine-grained nature of the material collected from Wild 2 indicates that it had not been lithified and altered in Wild 2 by internal processes such as heating, compaction or aqueous alteration (*3*). Although all particles were modified to some degree by capture in aerogel, particles that are larger than 1μm such as Coki are typically well-preserved and appear to have been protected by their own thermal inertia (*3*). We estimate that the distance Mg diffused in anorthite (using the diffusion coefficient of (*28*)) during the conditions of capture in aerogel (i.e. T ~2000 K, t >1μs (*3*)) is less than 1 nm.

We postulate that Coki formed by melting of solid precursor materials during transient high temperature events in the inner solar system analogous to type C CAIs and chondrules (*21, 29*). The chemical and isotopic data suggest that Coki is transitional between the only other CAI-like particle described from comet Wild 2, named Inti (*1, 3, 9*), and the chondrule-like objects from comet Wild 2 described by Nakamura et al. (*2*). As such, Coki may provide a direct link between primary CAI formation and later chondrule formation. Inti closely resembles type B CAIs in its mineralogy and ^{16}O-rich isotope composition (*1, 9*), whereas the ferromagnesian chondrule-like objects have less refractory chemical compositions and display a range of O-isotope compositions suggesting they experienced oxygen isotope exchange in a ^{16}O-depleted reservoir (*2*). These observations lead to the conclusion made in previous studies (*1-4*) that comet Wild 2 contains an abundance of chemically and thermally processed high temperature material from the inner solar system. In this sense, comet Wild 2 is analogous to carbonaceous chondrite meteorites (*5*).

As an additional member of the collection of refractory materials from comet Wild 2, Coki adds weight to the evidence suggesting that high temperature silicate and oxide mineral assemblages formed close to the Sun and were subsequently transported to the region of comet accretion. Coki provides a temporal constraint demonstrating that refractory material supplied to the Kuiper belt crystallized at least 1.7 million years after the onset of CAI formation. This observation in turn requires transport of inner solar system material to the outer reaches of the

solar system at distances exceeding 30 AU and incorporation into cometary bodies over an extended period of at least several million years. Outward transport of Coki to the Kuiper belt must have occurred as late as (if not later than) the time over which chondritic meteorites and the oldest differentiated meteorites formed (see *30*). The age constraint derived from Coki indicates that the transport mechanisms which supplied high-temperature inner solar system material to the outer reaches of the solar nebula, whether by lofting above the disk in an X-wind model (*31*) or via mixing processes within the solar nebula (e.g. *32*, *33*) , operated over a >2 million year timescale as solids settled to the midplane and the disk evolved.

REFERENCES AND NOTES

1. K. D. McKeegan *et al.*, *Science* **314**, 1724 (2006).
2. T. Nakamura *et al.*, *Science* **321**, 1664 (2008).
3. D. Brownlee *et al.*, *Science* **314**, 1711 (2006).
4. M. E. Zolensky *et al.*, *Science* **314**, 1735 (2006).
5. H. A. Ishii *et al.*, *Science* **319**, 447 (2008).
6. G. J. MacPherson, in *Meteorites, Comets and Planets: Treatise on Geochemistry, Volume 1*. (2005), pp. 201-245.
7. K. D. McKeegan, M. Chaussidon, F. Robert, *Science* **289**, 1334 (2000).
8. Y. Amelin, A. N. Krot, I. D. Hutcheon, A. A. Ulyanov, *Science* **297**, 1678 (2002).
9. S. B. Simon *et al.*, *Meteoritics & Planet. Sci.* **43**, 1861 (2008).
10. G. J. MacPherson, A. M. Davis, E. K. Zinner, *Meteoritics* **30**, 365 (1995).
11. M.-C. Liu *et al.*, *Geochim. Cosmochim. Acta* **73**, 5051 (2009).
12. G. J. Wasserburg, T. Lee, D. A. Papanastassiou, *Geophysical Research Letters* **4**, 299 (1977).

13. A description of the track from which Coki was recovered is available in the supporting online material.

14. G. J. MacPherson, G. R. Huss, *Geochimica et Cosmochimica Acta* **69**, 3099 (2005).

15. D. A. Wark, *Geochimica et Cosmochimica Acta* **51**, 221 (1987).

16. A. N. Krot *et al.*, *Geochim. Cosmochim. Acta* **71**, 4342 (2007).

17. Materials and methods are available as supporting material on Science online.

18. K. Thrane, M. Bizzarro, J. A. Baker, *Ap J* **646**, L159 (2006).

19. B. Jacobsen *et al.*, *EPSL* **272**, 353 (2008).

20. J. Villeneuve, M. Chaussidon, G. Libourel, *Science* **325**, 985 (2009).

21. A. N. Krot, H. Yurimoto, I. D. Hutcheon, G. J. MacPherson, *Nature* **434**, 998 (2005).

22. N. T. Kita, H. Nagahara, S. Togashi, Y. Morishita, *Geochim. Cosmochim. Acta* **64**, 3913 (2000).

23. G. R. Huss, G. J. MacPherson, G. J. Wasserburg, S. S. Russell, G. Srinivasan, *Meteoritics & Planet. Sci.* **36**, 975 (2001).

24. I. D. Hutcheon, K. K. Marhas, A. N. Krot, J. N. Goswami, R. H. Jones, *Geochim. Cosmochim. Acta* **73**, 5080 (2009).

25. S. S. Russell *et al.*, in *Meteorites and the Early Solar System II*, D. S. Lauretta, H. Y. McSween, Jr., Eds. (The University of Arizona Press, Tucson, 2006), pp. 233-251.

26. E. R. D. Scott, A. N. Krot, in *Chondrites and the Protoplanetary Disk* A. N. Krot, E. R. D. Scott, B. Reipurth, Eds. (2005), vol. 341, pp. 15-53.

27. A. N. Krot *et al.*, *Meteoritics & Planet. Sci.* **42**, 1197 (2007).

28. T. Latourrette, G. J. Wasserburg, *EPSL* **158**, 91 (1998).

29. R. H. Jones, T. Lee, H. C. Connolly, Jr., S. G. Love, H. Shang, in *Protostars and Planets IV*, V. Mannings, A. P. Boss, S. S. Russell, Eds. (The University of Arizona Press, Tuscson, 2000), pp. 927-962.

30. R. W. Carlson, M. Boyet, *EPSL* **279**, 147 (2009).

31. F. H. Shu, H. Shang, T. Lee, *Science* **271**, 1545 (1996).

32. F. J. Ciesla, *Science* **318**, 613 (2007).

33. A. P. Boss, *Ap J* **616**, 1265 (2004).

34. Y. J. Sheng, I. D. Hutcheon, G. J. Wasserburg, *Geochim. Cosmochim. Acta* **55**, 581 (1991).

35. This work was performed under the auspices of the U.S. Department of Energy by Lawrence Livermore National Laboratory under Contract DE-AC52-07NA27344. The work was supported by NASA grants #NNH07AG46I (H.A. Ishii) and #NNH04AB47I (I.D. Hutcheon), and LLNL grant #06-ERI-001 (J.P. Bradley).

Supporting Online Material

www.sciencemag.org

Materials and Methods

SOM text

Figures S1-S3

Tables S1-S3

References

Table 1. ^{26}Al-^{26}Mg isotopic data from Coki[¶].

Sample	$^{27}Al/^{24}Mg$	$\delta^{26}Mg$ (‰)[‖]
Coki 1[†]	342 ± 34	-17 ± 37
Coki 2[‡]	150 ± 15	18 ± 45
Coki 3[§]	6.9 ± 0.7	1.6 ± 6.5

[†]Includes pixels with $^{27}Al/^{24}Mg > 200$

[‡]Includes pixels with $^{27}Al/^{24}Mg$ between 100 and 200

[§]Includes pixels with $^{27}Al/^{24}Mg < 10$

[‖]Permil deviation in $^{26}Mg/^{24}Mg$ relative to terrestrial Mg after correction for mass-dependent fractionation. See supporting online material for details.

Uncertainties are two standard deviations.

FIGURE CAPTIONS

Figure 1. (A) Secondary electron image of the Coki section analyzed in this study showing mineral shards surrounded by compressed aerogel. (B) Corresponding false color mineral map overlaid on a montage of brightfield TEM images (*17*).

Figure 2. Coki pyroxene chemical compositions as compared to type C CAIs (*15-16*) and plagioclase-rich chondrules (*14, 16, 34*).

Figure 3. ^{26}Al-^{26}Mg evolution diagram for Coki. The solid horizontal line corresponds to terrestrial Mg. The dashed line indicates the canonical $^{26}Al/^{27}Al$ value of $5x10^{-5}$, while the dotted line represents the 2σ upper error bound on a line fitted to the data and forced through the origin corresponding to initial $^{26}Al/^{27}Al < 1x10^{-5}$.

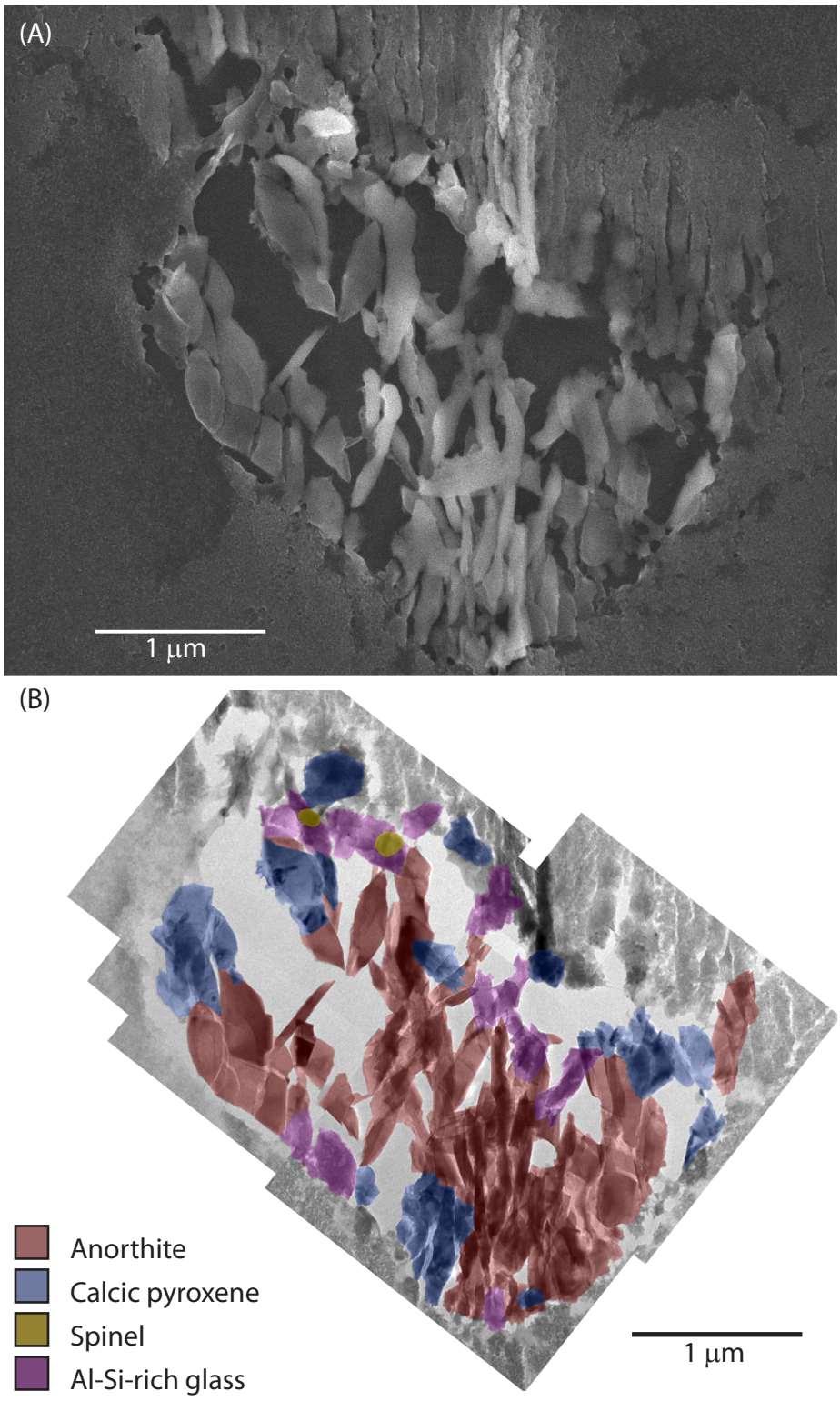
(A)
1 μm
(B)
Anorthite
Calcic pyroxene
Spinel
Al-Si-rich glass
1 μm

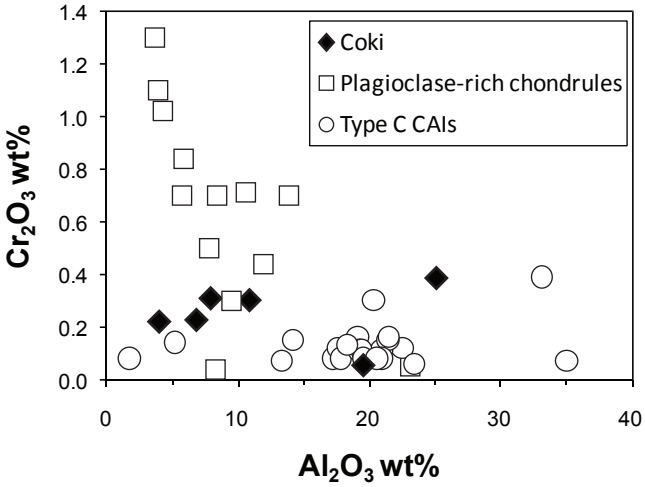
Coki
Plagioclase-rich chondrules
Type C CAIs
Cr_2O_3 wt%
Al_2O_3 wt%
0.0
0.2
0.4
0.6
0.8
1.0
1.2
1.4
0
10
20
30
40

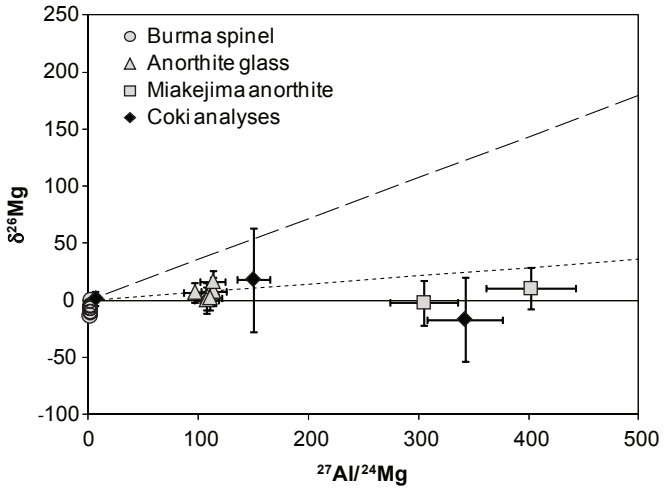
Burma spinel
Anorthite glass
Miakejima anorthite
Coki analyses
δ26Mg
27Al/24Mg
250
200
150
100
50
0
-50
-100
0
100
200
300
400
500

SUPPORTING ONLINE MATERIAL

MATERIALS AND METHODS

Transmission Electron Microscopy – Focused Ion Beam Sample Preparation and Measurements

The Coki-5-B track was compressed, embedded in acrylic resin (*1*), and electron transparent thin-sections were prepared from the Coki particle using an ultramicrotome with a diamond knife at the University of Washington. Sections 50-80 nm in thickness were mounted on continuous carbon substrates supported on 3 mm diameter Cu-mesh grids. The thin sections were examined using transmission electron microscopy, and mineral compositions (Table S1, Fig. S1) were determined by energy dispersive x-ray spectroscopy (EDS). Microscopes used in this work are two 200kV FEI Tecnai F20 field-emission scanning transmission electron microscopes ((S)TEM) each with a Gatan energy filter, EDAX Si(Li) solid state energy-dispersive X-ray detector and high angle annular dark field (HAADF) detector at the University of Washington and at Lawrence Livermore National Laboratory. Bright-field, dark-field imaging, diffraction, tilting experiments and EDS were used to locate and identify minerals present including (Mg-rich) spinel inclusions <200 nm in diameter. Mineral maps were produced by examining samples shard-by-shard using conventional TEM-EDS rather than by (S)TEM x-ray mapping to minimize any potential effects of electron beam damage.

After TEM characterization of Coki, an FEI Nova NanoLab 600 dual-beam focused ion beam (FIB) instrument at Lawrence Livermore National Laboratory was used to deposit ~10 μm wide and ~1 μm thick Pt ribbons behind the sample by interaction of first the electron, and then the ion, beam with a locally-injected organometallic gas. The Pt provides a conductive mechanical support allowing the fragile ultramicrotomed section to undergo NanoSIMS analysis. After back-coating the sample, a JEOL JSM-5800 LV secondary electron microscope (SEM) was used to generate high resolution images for correlation of Coki fragment topography with the TEM mineral map in order to identify pyroxene and

spinel locations. The 30 kV Ga^+ ion beam of the FIB instrument was then used to precisely and accurately mill away submicron-sized pyroxene fragments with a current of 30 pA (Figs. 1 and S2). The pyroxene was removed to mitigate dilution of the anorthite Mg isotopic signature by the surrounding pyroxene (*2*).

NanoSIMS Measurements

Isotope measurements were made by rastering a 3 pA O^- primary ion beam focused to a ~200 nm diameter spot over sample areas ranging in size from 2 x 2 μm^2 to 3 x 3 μm^2 until the sample was consumed. Images consist of up to 600 replicate scans of 32^2 pixels with a dwell time of 10 ms/pixel. Four ion images were simultaneously collected on electron multipliers corresponding to $^{24}Mg^+$, $^{25}Mg^+$, $^{26}Mg^+$ and $^{27}Al^+$ secondary ions. A mass resolving power of ~3700 was used to separate hydride or other interferences from the isotopes of interest.

Instrumental mass fractionation was accounted for by comparing the measured $^{25}Mg/^{24}Mg$ ratio of mineral standards with the $^{25}Mg/^{24}Mg$ of terrestrial Mg (0.12663, *3*) and is given in parts per thousand (permil, ‰) per amu by

$$\Delta^{25}Mg = [\{(^{25}Mg/^{24}Mg)_{meas}/0.12663\} - 1] \times 1000.$$

Standards analyzed in this study include Burma spinel, Miakejima plagioclase, and a synthetic anorthite composition glass. These standards provide a test of the NanoSIMS measurement because they have a range of Al/Mg concentrations and no radiogenic ^{26}Mg, and therefore they yield the same $^{26}Mg/^{24}Mg$ ratio relative to Al/Mg ratio. After correcting for instrumental mass fractionation using a linear law, the weighted average $^{26}Mg/^{24}Mg$ ratio of all terrestrial materials was 0.14227 ± 0.00012 (Table S2). The measured average $^{26}Mg/^{24}Mg$ is higher than the reference value of terrestrial Mg (0.13932, *3*) presumably because of differences in the gain between detectors. Any potential excess ^{26}Mg that

remained after correcting for mass fractionation is reported in permil relative to the measured $^{26}Mg/^{24}Mg$ of our standards:

$$\delta^{26}Mg = [\{(^{26}Mg/^{24}Mg)_{meas}/0.14227\} - 1] \times 1000.$$

The two analyses of Miakejima plagioclase were obtained from small (<3 μm) fragments that had been prepared in a manner identical to the Coki thin section. These analyses demonstrate that sample preparation did not bias the results.

Potential differences in ionization efficiency between Al and Mg were addressed by comparing the measured $^{27}Al^{+}/^{24}Mg^{+}$ to the "true" $^{27}Al/^{24}Mg$ of the anorthite composition. No correction to the measured $^{27}Al^{+}/^{24}Mg^{+}$ ratio was necessary.

We also analyzed two suites of isotopically-enriched synthetic glasses to test our ability to precisely and accurately measure deviations from the normal isotopic composition not due to mass dependent fractionation. These suites include two anorthite composition glass standards spiked with varying amounts of ^{25}Mg (*4*) and three pyroxene composition glass standards spiked with ^{26}Mg (K. McKeegan, unpublished data). The results from each standard agree well with gravimetrically calculated values (Table S3).

The Coki and Miakejima plagioclase data were processed as quantitative isotope ratio images using custom software (LIMAGE, L.R. Nittler). Each image was subdivided into regions based on the $^{27}Al/^{24}Mg$ ratio of individual pixels. The subdivision resulted in three spatially continuous regions (Fig. S3) corresponding to the three Coki data points in figure 3. The isotopic composition of each region was calculated by dividing the total counts of each isotope species in a given region and averaging the ratios over all of the replicate scans and all of the images. The reported error on the ratios is the 2σ standard error of the mean or the 2σ error based on counting statistics, whichever is larger.

MINERALOGY OF TRACK 141

Track #141 is a 2 mm long, type B track (*5*). The refractory particle, Coki, was one of the more competent and coarse fragments found along with two pyroxene fragments, an ~3 μm in diameter aggregate of Fe-rich olivine, augite and albite or albitic glass, and the terminal particle in the track, a ~5 μm in diameter pentlandite fragment with attached Fe-rich olivine and augite and glass. The bulbous, upper track contained the only identified presolar silicon carbide crystal in the Stardust materials (*6-7*). The genetic relationship between the fragments, if any, is unclear.

The possibility that Coki did not originate from Comet Wild 2, but was rather a passing interplanetary dust particle (IDP), is highly unlikely for several reasons. 1) CAI-like objects are very rare in IDPs. 2) There were no impacts of the size of the particle that generated track #141 on the interstellar side of the collector which supports our assertion that impacts from IDPs are very rare events. 3) Impacts from passing IDPs would be expected to produce randomly oriented tracks. However, no off-normal tracks were observed on the cometary side of the collector, and off-normal tracks seen on the interstellar side of the collector have been shown to have been produced by secondary debris from an impact with the spacecraft.

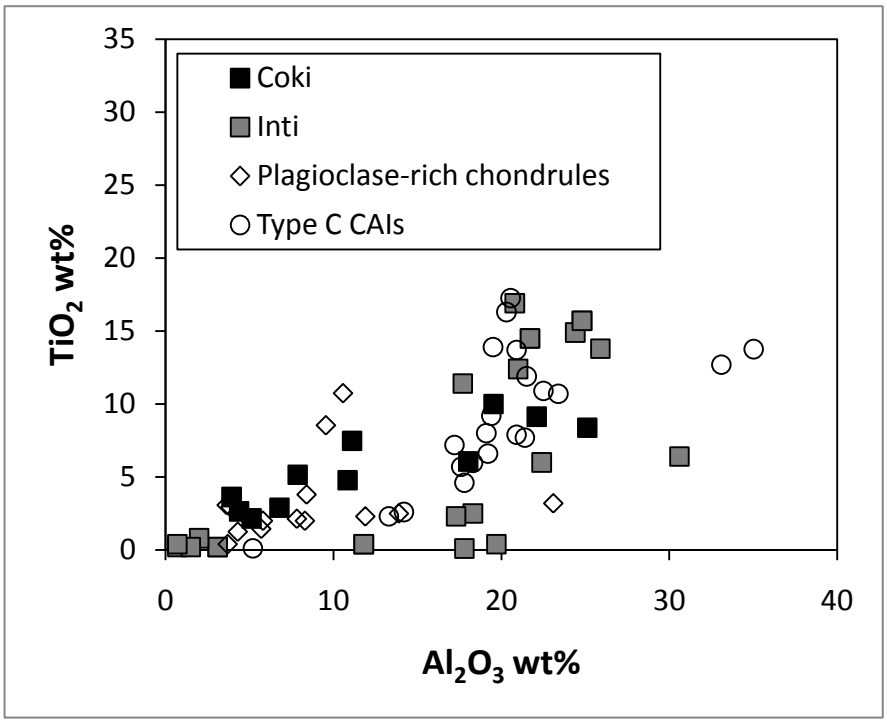

Figure S1. Coki pyroxene compositions as compared to type C CAIs (*8-9*), plagioclase-rich chondrules (*8, 10-11*), and Inti (*12*). Coki pyroxene compositions are Ca-, Al-, and Ti-rich relative to chondrule pyroxene compositions.

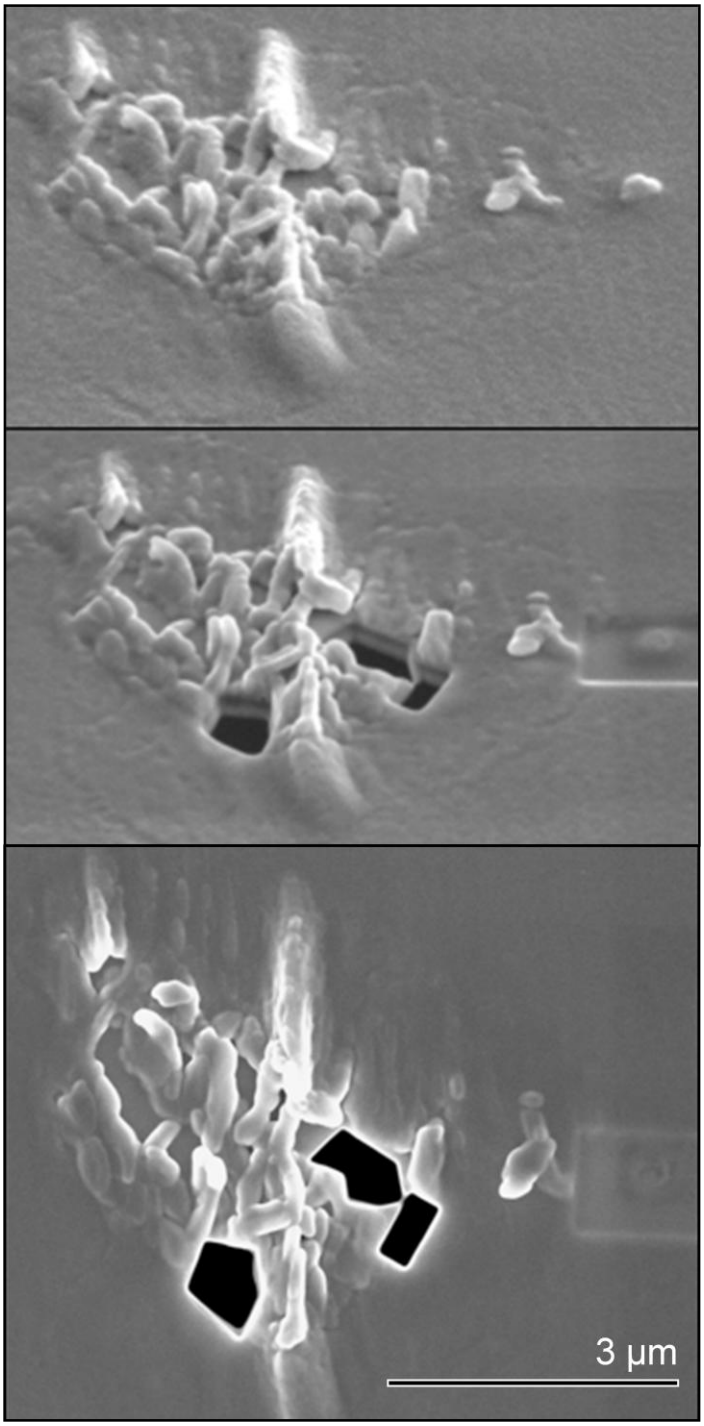

Figure S2. Removal of pyroxene fragments to mitigate dilution of anorthite Mg isotope signatures. Secondary electron images of the Coki particle thin section (top) at a tilt of 52° prior to any focused ion beam milling and (middle) at a tilt of 52° and (bottom) 0° after focused ion beam milling of selected pyroxene fragments. A rectangular region at the right containing a fragment of Na-augite was imaged by the ion beam for the purpose of focus and stigmation of the beam prior to milling.

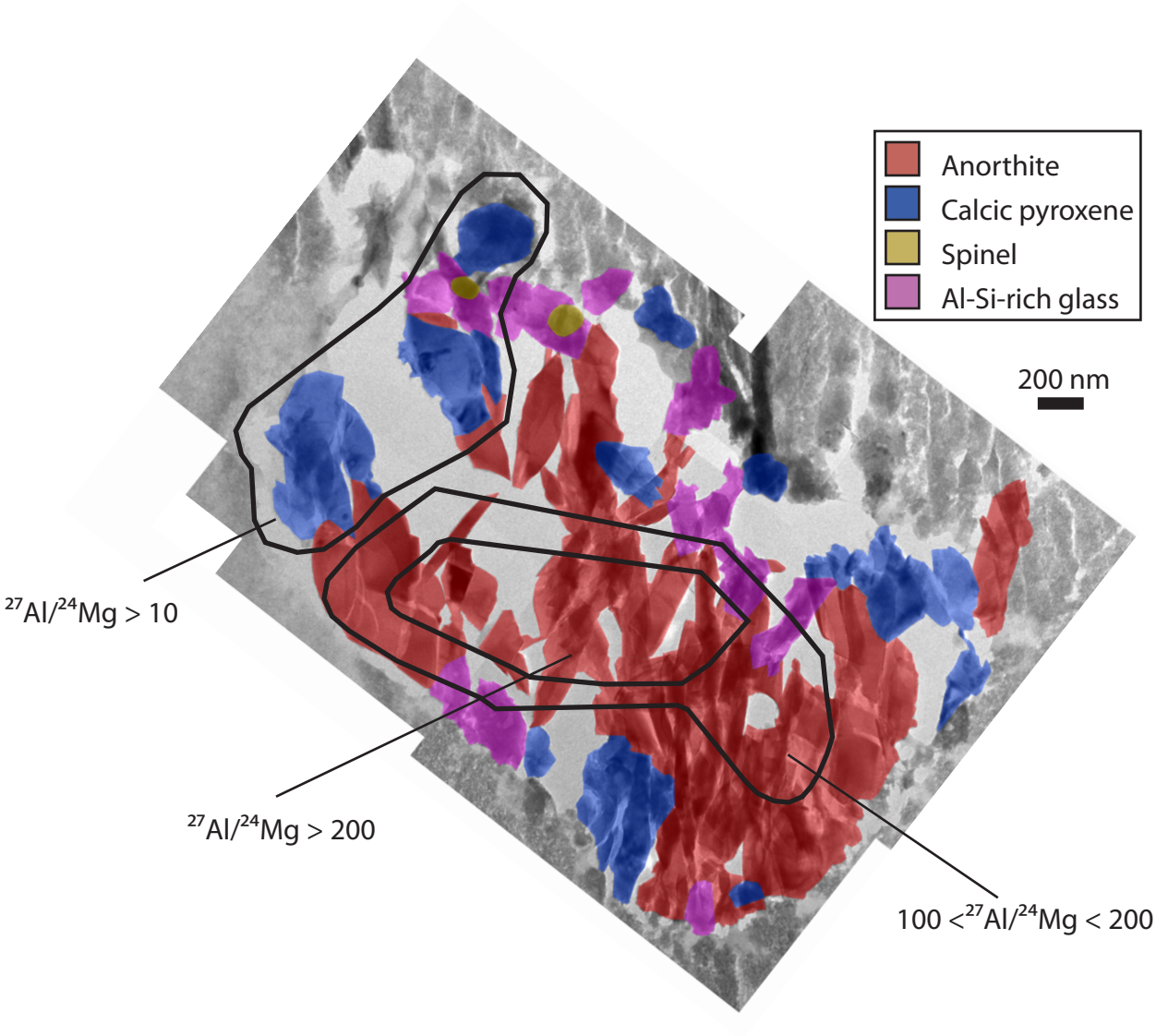

Figure S3. False color mineral map of the Coki section overlaid on a montage of brightfield TEM images. Heavy black lines outline the regions incorporated into each data point.

Table S1. Chemical compositions of Coki pyroxene and anorthite determined by TEM/EDS.

Mineral	pyroxene											anorthite		
Spot Number	UW -1	UW -2	UW -3	UW -4	UW -5	UW -6	LLNL -1	LLNL -2	LLNL -3	LLNL -4	LLNL -5	LLNL -1	LLNL -2	LLNL -3
SiO_2	37.6	56.1	54.6	45.6	45.7	45.0	43.9	41.8	53.7	40.9	50.3	41.7	43.2	41.8
TiO_2	10.0	2.6	3.6	5.2	4.8	7.5	9.1	6.1	2.2	8.4	2.9	n.m.	n.m.	n.m.
Al_2O_3	19.5	4.4	3.9	7.9	10.8	11.1	22.1	18.0	5.1	25.1	6.8	37.0	36.7	38.9
Cr_2O_3	0.1	n.d.	0.2	0.3	0.3	n.d.	n.d.	n.d.	n.d.	0.4	0.2	n.m.	n.m.	n.m.
FeO	n.d.	0.3	0.2	0.4	0.3	0.2	n.d.	n.d.	n.d.	n.d.	n.d.	n.m.	n.m.	n.m.
V_2O_3	n.d.	n.d.	n.d.	0.2	0.3	0.3	n.m.	n.m.	n.m.	n.m.	n.m.	n.m.	n.m.	n.m.
MgO	8.4	16.4	15.4	16.4	14.1	12.5	6.9	10.0	20.0	8.4	16.1	n.m.	n.m.	n.m.
CaO	24.4	20.2	22.0	24.0	23.6	23.4	18.0	24.2	19.0	16.6	23.5	21.3	20.2	19.3

Analyses are normalized to 100 wt% oxides. Relative uncertainties (1σ) based on counting statistics are <5% for SiO_2, Al_2O_3, MgO, CaO <15% for TiO_2, and <30% for V_2O_3, Cr_2O_3, and FeO. n.m.: not measured; n.d.: not detected

Table S2. Isotope data from terrestrial standards.

Standard	**n†**	**$^{25}Mg/^{24}Mg$‡**	**$^{26}Mg/^{24}Mg$¥**	**$^{27}Al/^{24}Mg$**
Anorthite glass	6	0.12390 ± 0.00026	0.14325 ± 0.00061	108 ± 4.4
Miakejima plagioclase	2	0.12367 ± 0.00086	0.14291 ± 0.00191	340 ± 24
Burma spinel	8	0.12445 ± 0.00005	0.14223 ± 0.00012	2.0 ± 0.1
Weighted mean			0.14227 ± 0.00012	

†Number of analyses

‡Mean and 2σ uncertainty of n measurements.

¥Fractionation corrected $^{26}Mg/^{24}Mg$ (assuming linear fractionation law and $^{25}Mg/_{24}Mg = 0.12663$). Uncertainties are 2$\sigma$.

Table S3. Mg isotope data from isotopically enriched standards.

Standard	n[†]	δ^{26}Mg (‰)[‡]	δ^{26}Mg (‰) by gravimetry	δ^{25}Mg (‰)[¥]	δ^{25}Mg (‰) by gravimetry
P0	6	0.0 ±0.7	0.0	–	–
P10	3	10 ±0.9	10.05	–	–
P99	3	99 ±1.1	99.0	–	–
AnMg-6	1	–	–	9.5 ±6.0	9.4
AnMg-8	1	–	–	97 ±8.2	97.9

[†]Number of analyses

[‡]^{26}Mg-enrichment after correcting for mass fractionation (assuming linear fractionation law and ^{25}Mg/^{24}Mg = 0.12663) reported in permil relative to terrestrial Mg.

[¥]^{25}Mg-enrichment after correcting for mass fractionation (assuming linear fractionation law and ^{26}Mg/^{24}Mg = 0.13932) reported in permil relative to terrestrial Mg.

REFERENCES

1. G. Matrajt, D. E. Brownlee, *Meteoritics & Planet. Sci.* **41**, 1715 (2006).
2. H. A. Ishii *et al.*, *Proceedings of the Lunar and Planetary Science Conference* **40**, 2288 (2009).
3. E. Catanzaro, T. Murphy, E. Garner, W. Shields, *Journal of Research of the National Bureau of Standards* **70A**, 453 (1966).
4. J. T. Armstrong, J. C. Huneke, H. F. Shaw, T. A. Finnerty, G. J. Wasserburg, in *Microbeam Analysis - 1982,* K. F. J. Heinrich, Ed. (San Francisco Press, San Francisco, 1982), pp. 205-209.
5. F. Hörz *et al.*, *Science* **314**, 1716 (2006).
6. D. E. Brownlee, D. Joswiak, G. Matrajt, S. Messenger, M. Ito, in *Lunar and Planetary Institute Science Conference Abstracts*. (2009), vol. 40, pp. 2195.
7. S. Messenger, D. Joswiak, M. Ito, G. Matrajt, D. E. Brownlee, in *Lunar and Planetary Institute Science Conference Abstracts*. (2009), vol. 40, pp. 1790.
8. A. N. Krot *et al.*, *Geochim. Cosmochim. Acta* **71**, 4342 (2007).
9. D. A. Wark, *Geochim. Cosmochim. Acta* **51**, 221 (1987).
10. G. J. MacPherson, G. R. Huss, *Geochim. Cosmochim. Acta* **69**, 3099 (2005).
11. Y. J. Sheng, I. D. Hutcheon, G. J. Wasserburg, *Geochim. Cosmochim. Acta* **55**, 581 (1991).
12. S. B. Simon *et al.*, *Meteoritics & Planet. Sci.* **43**, 1861 (2008).